Photoinduced transformations of stiff-stilbene-based discrete metallacycles to metallosupramolecular polymers

Xuzhou Yan[a,b], Jiang-Fei Xu[c], Timothy R. Cook[b], Feihe Huang[a,1], Qing-Zheng Yang[c,1], Chen-Ho Tung[c], and Peter J. Stang[b,1]

[a]State Key Laboratory of Chemical Engineering, Department of Chemistry, Zhejiang University, Hangzhou, Zhejiang 310027, People's Republic of China; [b]Department of Chemistry, University of Utah, Salt Lake City, UT 84112; and [c]Key Laboratory of Photochemical Conversion and Optoelectronic Materials, Technical Institute of Physics and Chemistry, Chinese Academy of Sciences, Beijing 100190, People's Republic of China

Contributed by Peter J. Stang, May 12, 2014 (sent for review April 2, 2014)

Control over structural transformations in supramolecular entities by external stimuli is critical for the development of adaptable and functional soft materials. Herein, we have designed and synthesized a dipyridyl donor containing a central *Z*-configured stiff-stilbene unit that self-assembles in the presence of two 180° di-Pt(II) acceptors to produce size-controllable discrete organoplatinum(II) metallacycles with high efficiency by means of the directional-bonding approach. These discrete metallacycles undergo transformation into extended metallosupramolecular polymers upon the conformational switching of the dipyridyl ligand from *Z*-configured (0°) to *E*-configured (180°) when photoirradiated. This transformation is accompanied by interesting morphological changes at nanoscopic length scales. The discrete metallacycles aggregate to spherical nanoparticles that evolve into long nanofibers upon polymer formation. These fibers can be reversibly converted to cyclic oligomers by changing the wavelength of irradiation, which reintroduces *Z*-configured building blocks owing to the reversible nature of stiff-stilbene photoisomerization. The design strategy defined here represents a novel self-assembly pathway to deliver advanced supramolecular assemblies by means of photocontrol.

metal coordination | supramolecular coordination complex | photoirradiation | reversibility | dynamic materials

Natural systems provide many examples of self-assembled biosupramolecules that respond to external stimuli through conformational changes that ultimately play a role in carrying out their various biological functions. Mimicking this stimuli-responsive behavior in artificial systems is a promising route toward obtaining sophisticated molecular-based architectures with functional and structural tunability (1–3). Using the absorption of photons as a trigger is particularly attractive in that light-induced transformations maintain high spatial and temporal resolution without producing waste products even during multiple reversible switching sequences (4). In materials science, one of the most appealing characteristics of photochromic molecules is the direct conversion of light into mechanical energy based on their photo-reversible structural transformations (5). Among such chromophores, a stiff-stilbene moiety (1,1′-biindane) is useful owing to its unique characteristics (6). First, stiff stilbene can adopt either a *cis* or *trans* configuration with respect to its central double bond. Second, the high activation barrier between the two isomers (~43 kcal·mol^{-1}, corresponding to a half-life of ~10^9 y at 300 K) makes thermal *E*/*Z* isomerization negligible at temperatures of 420 K and lower. Third, the quantum yield for the photoisomerization of either isomer is high (50%). Fourth, the stiff-stilbene core is readily substituted using well-established synthetic methods. Owing to these promising characteristics, Boulatov and coworkers (7) constructed a molecular force probe by integrating the moiety into a stretched polymer to mimic the strain generated in diverse functional groups. Yang and coworkers (8) reported hydrogen-bonded supramolecular polymers and studied their polymerization mechanisms and physical properties based on the photoisomerization of the stiff-stilbene units. Nevertheless, stiff-stilbene-based supramolecular entities are underexplored despite exhibiting properties that make the functionality potentially useful in the construction of photoresponsive supramolecular materials.

Coordination-driven self-assembly is a powerful method of constructing supramolecular coordination complexes (SCCs) by the spontaneous formation of metal–ligand bonds that draws inspiration from the design principles of natural systems (9–20). This approach organizes metal acceptors and organic donors to prepare well-defined cavity-cored 2D metallacycles and 3D metallacages, which can be functionalized on their interior or exterior vertices for applications in host–guest chemistry (21, 22), catalysis (23), molecular flasks (24), bioengineering (25), amphiphilic self-assembly (26), and so on. The versatility of coordination-driven self-assembly can be enhanced by designs that allow for post-self-assembly modifications that in some cases result in complete structural transformations. For example, the Stang group previously demonstrated the transformation of self-assembled polygons by changing the angle between the bonding sites of a ligand from 180° to 120° upon treatment of $Co_2(CO)_6$ with an acetylene moiety (27). Yang and coworkers (28) reported the construction of multibisthienylethene hexagons capable of reversible supramolecule-to-supramolecule conversions induced by ring-open and ring-closed conformational changes of the bisthienylethene units. Herein we expand upon the transformations

Significance

Coordination-driven self-assembly is a synthetic method used to generate complex structures based on the simple formation of metal–ligand bonds between molecular building blocks. These building blocks can be functionalized in a variety of ways, endowing the process with a wide range of modularity and tunability. Here, a building block is used that changes its structure when it absorbs light. Because the geometry of each building block is a critical determinant of overall structure, when the precursor changes its shape the final assembly transforms from a discrete metallacycle to an extended 1D network. This technique demonstrates that coordination-driven self-assembly can be used to obtain dynamic materials that respond to external stimuli.

Author contributions: X.Y., J.-F.X., F.H., Q.-Z.Y., and P.J.S. designed research; X.Y. and J.-F.X. performed research; X.Y. contributed new reagents/analytic tools; X.Y., J.-F.X., T.R.C., and Q.-Z.Y. analyzed data; and X.Y., T.R.C., F.H., Q.-Z.Y., C.-H.T., and P.J.S. wrote the paper.

The authors declare no conflict of interest.

[1]To whom correspondence may be addressed. E-mail: fhuang@zju.edu.cn, qzyang@mail.ipc.ac.cn, or stang@chem.utah.edu.

This article contains supporting information online at www.pnas.org/lookup/suppl/doi:10.1073/pnas.1408620111/-/DCSupplemental.

established by the systems described above designing SCCs capable of evolving from discrete metallacycles into infinite constructs using external stimuli.

Supramolecular polymers can be defined as dynamically reversible polymeric arrays (29–37) that form from the explicit manipulation of noncovalent forces between monomeric units (38–43). Supramolecular polymer chemistry can readily complement coordination-driven self-assembly, as exemplified by our efforts to design hierarchical supramolecular polymerizations of discrete organoplatinum(II) metallacycles, thus accessing novel supramolecular polymeric materials, such as macroscopic hexagonal supramolecular polymer fibers (44), dendronized organoplatinum(II) metallacyclic polymers (45), and a responsive, cavity-cored supramolecular polymer network metallogel (46). Herein, we report photoresponsive supramolecular transformations between discrete organoplatinum(II) metallacycles and infinite metallosupramolecular polymers induced by a *cis*/*trans* conformational transition of a stiff-stilbene-based dipyridyl ligand. The self-assembly behaviors, physical properties, topologies, and morphologies of these SCCs can be regulated by photoisomerization, demonstrating this powerful approach to prepare advanced supramolecular coordination complexes.

Results and Discussion

The dipyridyl ligand *Z*-**1** can be readily synthesized by nucleophilic substitution of 1,1′-biindenylidene diol with 4-(chloromethyl) pyridine hydrochloride in 75% isolated yield (*SI Appendix*, *Scheme S1*). The *cis* nature of the *Z*-**1** isomer renders it a 0° donor based on the tenets of the directional bonding approach. Upon mixing with complementary 180° di-Pt(II) acceptors, two discrete metallacycles of varied size can be obtained via coordination-driven self-assembly. Irradiation of *Z*-**1** at 387 nm generates its corresponding *trans* isomer, *E*-**1**, in almost quantitative yield. This isomerization changes the ligand into a 180° donor (Fig. 1*A*). Whereas the *cis* form yields closed metallacycles upon self-assembly, the 180° form does not produce convergent geometries, instead furnishing linear metallosupramolecular polymers. The ready accessibility of both isomers of ligand **1** makes a detailed investigation of the photoresponsive supramolecular transformation between discrete metallacycles (DMCs) and infinite metallosupramolecular polymers (MSPs) possible.

Stirring equimolar mixtures of *Z*-**1** with either acceptor **2** or **3** in CD_2Cl_2 at room temperature for 8 h leads to the formation of self-assembled discrete metallacycles **4** and **5**, respectively (Fig. 1*B* and *SI Appendix*, *Schemes S2* and *S3*). Multinuclear NMR (^{1}H and ^{31}P) analysis of **4** and **5** support the formation of discrete metallacycles with highly symmetric structures (Fig. 2). For example, the $^{31}P\{^1H\}$ NMR spectra of **4** and **5** show sharp singlets (*ca.* 12.79 ppm for DMC **4** and 13.49 ppm for DMC **5**) with concomitant ^{195}Pt satellites ($J_{Pt\text{-}P}$ = 2,725.0 Hz for DMC **4** and $J_{Pt\text{-}P}$ = 2,692.6 Hz for DMC **5**) indicative of a single phosphorous environment (Fig. 2, spectra *B* and *D*). The peaks are shifted upfield relative to those of precursors **2** and **3** by ∼6.25 ppm. In addition, in the ^{1}H NMR spectrum of DMC **4** (Fig. 2, spectrum *F*), the proton signals of the pyridine rings showed downfield shifts ($\Delta\delta[H_\alpha]$ = 0.09 ppm; $\Delta\delta[H_\beta]$ = 0.49 ppm) compared with those of *Z*-**1** (Fig. 2, spectrum *G*), consistent with the loss of electron density that occurs upon pyridyl coordination with the acceptor. Similarly, in the ^{1}H NMR spectrum of DMC **5** (Fig. 2, spectrum *H*), the *α*- and *β*-pyridyl hydrogen signals both shift downfield ($\Delta\delta[H_\alpha]$ = 0.11 ppm; $\Delta\delta[H_\beta]$ = 0.51 ppm), owing to coordination.

The stoichiometry of formation of metallacycles **4** and **5** was confirmed by electrospray ionization (ESI) time of flight MS, which allows for the observation of peaks corresponding to intact assemblies with high isotopic resolution. In the mass spectrum of DMC **4**, five peaks were consistent with our assignment of a [2 + 2] assembly (*SI Appendix*, Fig. S6). Among these were a peak at

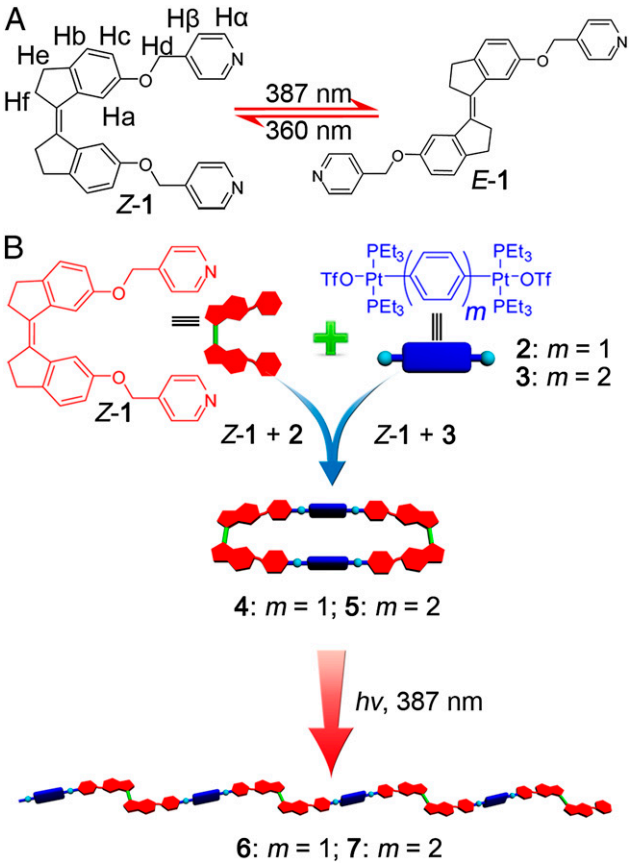

Fig. 1. Photoisomerization of the ligand and discrete metallacycles. (*A*) Reversible photoisomerization of the pyridine-linked stiff-stilbene derivatives *Z*-**1** and *E*-**1**. (*B*) Cartoon representation of the formation of discrete organoplatinum(II) metallacycles **4** and **5** and infinite metallosupramolecular polymers **6** and **7**.

m/*z* 702.77 corresponding to $[M - 3OTf - HOTf + K]^{4+}$. For DMC **5**, five such peaks were also found (*SI Appendix*, Fig. S9), such as the peaks at *m*/*z* 740.78 corresponding to $[M - 3OTf - HOTf + K]^{4+}$ and *m*/*z* 1,037.69 corresponding to $[M - 2OTf - HOTf + K]^{3+}$. All of the peaks were isotopically resolved and in good agreement with their calculated theoretical distributions, which allowed for the molecularity of the DMCs to be unambiguously established.

The transformation process triggered by photoirradiation of the two DMCs **4** and **5** was studied in CH_2Cl_2 at room temperature. In the ^{1}H NMR spectrum of DMC **4**, three sets of signals corresponding to protons H_a, H_e, and H_f on the stiff-stilbene unit were located at 7.58, 2.83, and 2.73 ppm, respectively (Fig. 3, spectrum *A*). Upon UV irradiation at 387 nm, the three peaks appeared at 7.20 ppm ($\Delta\delta[H_a]$ = 0.38 ppm), 3.13 ppm ($\Delta\delta[H_e]$ = 0.30 ppm), and 3.03 ppm ($\Delta\delta[H_f]$ = 0.30 ppm), respectively, which can be attributed to the resulting *E*-configured ligand (Fig. 3, spectrum *B*). Upon irradiation, the *α*- and *β*-pyridyl hydrogen signals show downfield shifts. These spectral changes in the ^{1}H NMR spectroscopy support the transformation of **4** into **6** as the directionality of the ligand changes from 0 to 180° (Fig. 1*B*). Similar features in the ^{1}H NMR spectra resulting from the structural transformation process of **1** were also observed for DMC **5** and MSP **7** (Fig. 3, spectra *C* and *D*). Despite these observable changes in the ^{1}H NMR spectra, no significant changes are notable in the $^{31}P\{^1H\}$ NMR spectra of either system (*SI Appendix*, Fig. S10), suggesting that the phosphorus

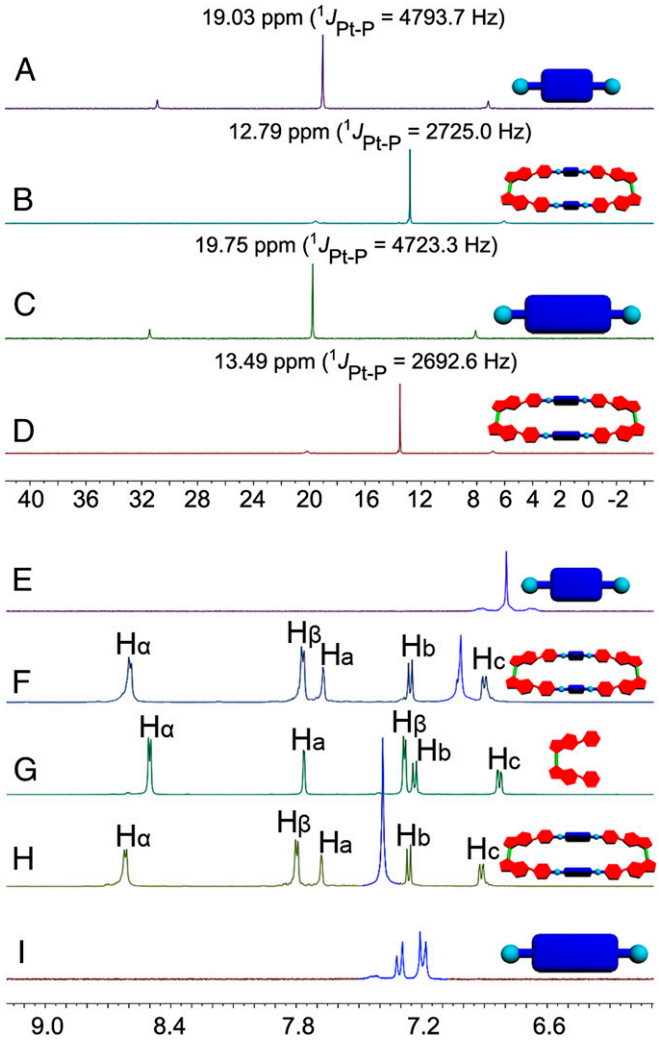

Fig. 2. NMR characterization of the formation of discrete metallacycles. Partial (*A–D*) ^{31}P and (*E–I*) ^{1}H NMR spectra (CD_2Cl_2, 293 K) of free building blocks *Z*-**1** (G), **2** (*A* and *E*), and **3** (*C* and *I*) and discrete metallacycles **4** (*B* and *F*) and **5** (*D* and *H*).

environments are not affected by the distant isomerization that has little bearing on the Pt–N bonding.

The structural transformations of **4** and **5** also manifested in changes to their absorption and emission properties. The UV-visible spectrum of DMC **4** showed a broad absorption band at ~350 nm, which is similar to that of the parent *Z*-stiff stilbene (Fig. 4*A*). Upon irradiation of **4** at 387 nm, two new absorption bands at *ca.* 342 and 358 nm were observed, arising from the corresponding photostationary state of the *E*-configured stiff-stilbene chromophore of MSP **6** (Fig. 4*A*). Similarly, irradiation of DMC **5** at 387 nm in CH_2Cl_2 also resulted in the *cis–trans* isomerization (Fig. 4*A*), prompting a transformation from DMC **5** to MSP **7**. Furthermore, the fluorescence spectra of **4** and **5** both showed an emission band at *ca.* 430 nm, which originates from the *Z*-configured stiff-stilbene unit (Fig. 4*B*). After transformation into MSPs, strong fluorescence enhancement occurred. From DMC **4** to MSP **6**, a *ca.* sixfold fluorescence enhancement was observed. Similarly, from DMC **5** to MSP **7**, a *ca.* ninefold fluorescence enhancement was observed. These spectral changes reveal that in addition to structural changes marked photophysical changes can be induced in stimuli-responsive materials.

The changes observed in the ^{1}H NMR, absorption, and emission spectra all support that the photoinduced structural transformation relies on the efficient *cis*/*trans* isomerization of the stiff-stilbene core. The transformation from discrete to extended structures likely occurs via one of two pathways. Although coordination to Pt suggests that the stiff-stilbene unit is locked in place, coordination-driven self-assembly relies on dynamic metal–ligand bonding. As such, minor amounts of dissociation between the Pt and pyridyl groups would allow for facile isomerization, after which coordination can reoccur. Alternatively, photon absorption would provide energetic input and strain on the SCC core, thereby providing impetus for Pt–N bond dissociation. As the core isomerizes, distorting the metallacycle, dissociation may occur, allowing the system to relax back to a thermodynamic minimum with a new configuration. As the metal–ligand bonds reform, an extended network would be generated.

To further confirm the photoinduced formation of MSPs, 2D diffusion-ordered ^{1}H NMR spectroscopy (DOSY) was performed to evaluate the metal coordination-driven supramolecular polymerization. The measured weight average diffusion coefficients of DMCs **4** and **5** were found to be 2.00×10^{-10} and 1.82×10^{-10} $m^2 \cdot s^{-1}$, respectively. However, after irradiation of **4** and **5** in CD_2Cl_2, the corresponding coefficients decreased to 7.94×10^{-11} and 5.01×10^{-11} $m^2 \cdot s^{-1}$, respectively (Fig. 4*C*). Furthermore, the concentration dependence of the measured weight-average diffusion coefficients of MSPs **6** and **7** has been determined. Upon increasing concentrations from 1 mM to 5 mM, the measured weight-average diffusion coefficients decreased from 9.83×10^{-10} to 7.94×10^{-10} $m^2 \cdot s^{-1}$ for MSP **6** and 7.21×10^{-10} to 5.01×10^{-10} $m^2 \cdot s^{-1}$ for MSP **7** (*SI Appendix*, Fig. S11). These significant decreases in average diffusion coefficient implied that large polymeric aggregates MSPs **6** and **7** formed after irradiation. Notably, the average diffusion coefficient of MSP **7** is smaller than that of MSP **6** ($D_{MSP\ 6}/D_{MSP\ 7} = 1.58$), indicating that the longer di-Pt(II) acceptor **3** results in larger MSP formation than that of its shorter counterpart. Moreover, dynamic light scattering (DLS) experiments were performed to provide further evidence for the formation of MSPs from DMCs. The average hydrodynamic diameters (D_h) of DMCs **4** and **5** were determined to be 2.70 and 3.12 nm, respectively, which can be attributed to the individual DMCs, as confirmed by molecular modeling (*SI Appendix*, Fig. S12). After irradiation of DMCs **4** and **5** in CH_2Cl_2 (1.00 mM), the corresponding D_h values

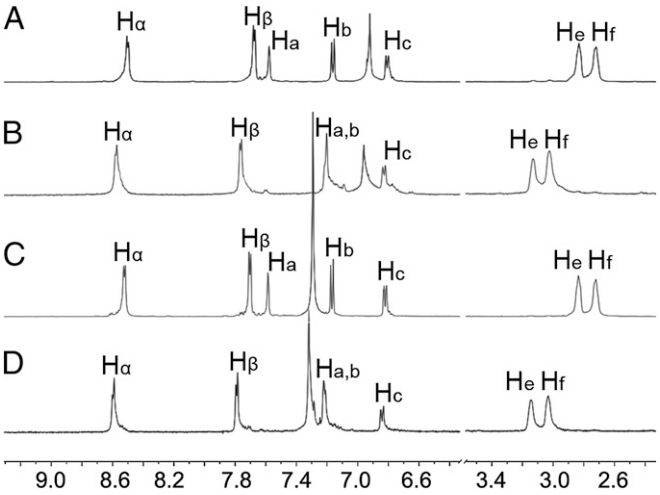

Fig. 3. Partial ^{1}H NMR spectra (CD_2Cl_2, 293 K, 500 MHz): (*A*) discrete metallacycle **4**, (*B*) metallosupramolecular polymer **6**, (*C*) discrete metallacycle **5**, and (*D*) metallosupramolecular polymer **7**. c = 5.00 mM.

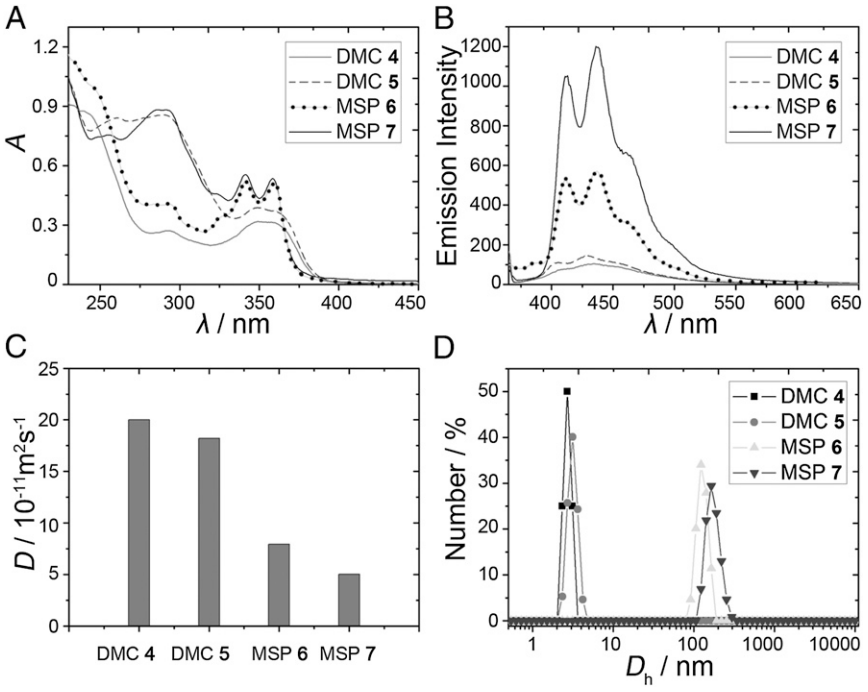

Fig. 4. Spectral characterization of the transformation from DMCs to MSPs. (*A*) UV-visible spectra of DMCs before and after irradiation at 387 nm (c = 20.0 μM). (*B*) Fluorescence spectra of DMCs before and after irradiation at 387 nm (λ_{ex} = 365 nm; c = 20.0 μM). (*C*) Diffusion coefficient D (CD_2Cl_2, 293 K, 500 MHz) of DMCs **4** and **5** and MSPs **7** and **8** (c = 5.00 mM). (*D*) Size distributions of DMCs before and after irradiation at 387 nm (c = 1.00 mM).

increased to 122.4 and 164.2 nm (Fig. 4*D*), respectively. When the initial concentrations of DMCs **4** and **5** in CH_2Cl_2 were increased to 2.00 mM, the corresponding D_h values increased to 342.0 and 396.2 nm, respectively, after irradiation (*SI Appendix*, Fig. S13). This increase is consistent with the formation of long metallosupramolecular polymer chains whose aggregate size is concentration-dependent. At higher concentrations, single chains are more likely to combine into larger groups of fibers, resulting in the observed DOSY and DLS data.

As evidenced above, 387-nm light irradiation produced MSPs. The reverse isomerization can be achieved by irradiation at 360 nm because this wavelength will reverse the *cis*/*trans* isomerization. Irradiation of **7** at 360 nm resulted in the formation of a mixture of *E*- and *Z*-configured species with a ratio of 47:53, as determined by ^{1}H NMR spectroscopy (*SI Appendix*, Fig. S14, spectrum *B*). Similar results have been observed for overcrowded alkenes systems developed by Qu and Feringa (47). The presence of the *Z*-configured isomer acts as a polymerization inhibitor, introducing a nonlinear angularity. Because not all of the ligand converts, quantitative formation of discrete metallacycles does not occur. Instead, the angled ligand is incorporated into larger cyclic oligomers as evidenced by a decrease in size based on DLS experiments (Fig. 5). The D_h value of MSP **7** at 1.00 mM was determined to be 164.2 nm. After irradiation at 360 nm, the corresponding D_h value decreased into 10.1 nm (*SI Appendix*, Fig. S15*A*), greatly disrupting the extended chain network to give significantly smaller species. This transformation can be reversed by irradiating at 387 nm, converting the stiff stilbene back to its linear form (Fig. 5). Fluorescence spectroscopy further supports the reversibility of this process, showing that repeated cycles of 360-nm and 387-nm exposures induce transitions between MSPs and cyclic oligomers (Fig. 6).

The morphological ramifications of the photoinduced transformations were explored using transmission electron microscopy (TEM). As shown in Fig. 7*A*, a TEM image of DMC **4** in CH_2Cl_2 revealed spherical nanoparticles with diameters that ranged from 10.0 to 80.0 nm, which can be attributed to the self-aggregation of the discrete metallacycles. When solutions of DMC **4** were irradiated by UV light at 387 nm, TEM images of the material showed remarkable morphological changes. Images of MSP **6** show that the extended network adopts a fibrous nanostructure (Fig. 7*C*). The nanofiber has a width of *ca.* 50.0 nm and a length of >1.00 μm, indicating a 1D propagation process. Similar morphological changes were also observed when DMC **5** transformed to MSP **7** (Fig. 7, *B* and *D*). These fibers represent bundles of single supramolecular polymer chains. Once the photoresponsive transformation of DMCs to MSPs occurs, these single metallosupramolecular polymeric chains aggregate and then further entangle to form associated clusters that ultimately self-assemble into nanofibers. Therefore, upon irradiating the discrete metallacycles in solution with UV light, an interesting morphological change between

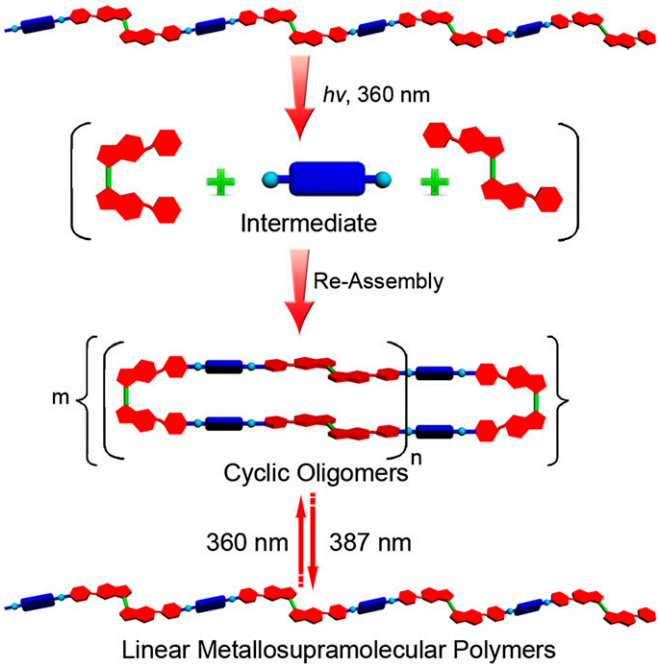

Fig. 5. Cartoon representation of the photoinduced reversible transformations between MSPs and cyclic oligomers.

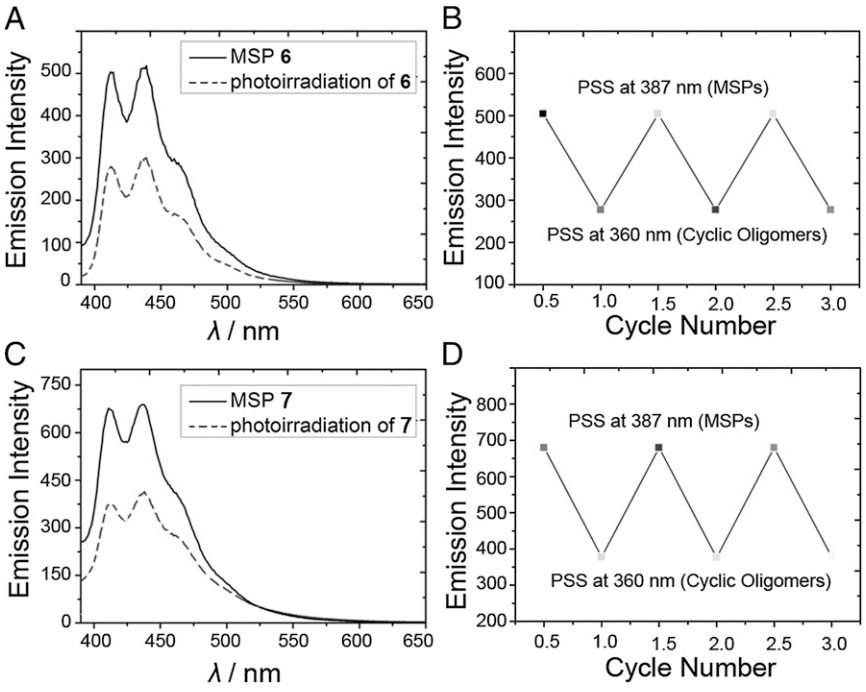

Fig. 6. Fluorescence characterization of the reversible transformations between MSPs and cyclic oligomers. Fluorescence spectra of MSPs **6** (*A*) and **7** (*C*) before and after irradiation at 360 nm (λ_{ex} = 365 nm; c = 10.0 μM). Cyclic changes in the emission intensity of MSPs **6** (*B*) and **7** (*D*) upon alternative irradiation at 360 nm and 387 nm.

nanoparticles and nanofibers was realized, indicating the dynamic nature of the SCCs.

Conclusion

A pyridyl-based ligand built upon a stiff-stilbene core was synthesized and used in self-assembly reactions with two 180° di-Pt(II) acceptors to produce two discrete metallacycles with high efficiency by means of a directional-bonding approach. These discrete metallacyclic precursors could be extended into infinite metallosupramolecular polymers upon photoinduced conformational transitions of the stiff-stilbene core from *Z* to *E* configuration, thus switching the ligand from a 0° to a 180° donor. Absorption of a photon either isomerizes dissociated ligands in solution that can then rebind to a metal center or induces structural changes of the metallacycle, prompting dissociation and transformation into an extended polymer. This process results in a structural change from discrete metallacycles to 1D chains, representing a novel route to photocontrolled supramolecular transformations. Moreover, the reversible nature of stiff-stilbene isomerization makes photoinduced structural transformations between high-molecular-weight MSPs and low-molecular-weight cyclic oligomers feasible. This work established new methods toward combining coordination-driven self-assembly, supramolecular polymerization, and stimuli-responsive soft materials and motivates ongoing efforts exploring new approaches to molecular materials with dynamic and controllable properties stemming from the incorporation of interesting functionalities into unique building blocks.

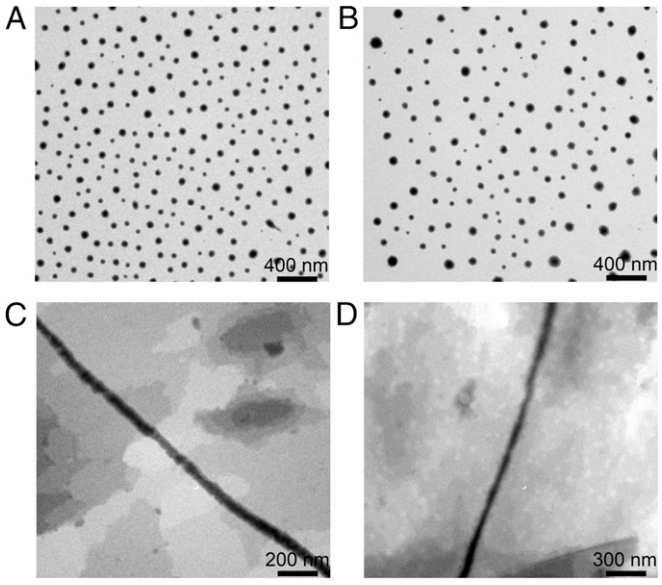

Fig. 7. (*A* and *B*) TEM images of nanoparticles formed by self-assembly of DMCs **4** and **5** in CH_2Cl_2. (*C* and *D*) TEM images of nanofibers formed by irradiation of the solutions of DMCs **4** and **5** in CH_2Cl_2. $c = 1.00 \times 10^{-4}$ M.

Materials and Methods

All reagents were commercially available and used as supplied without further purification. Deuterated solvents were purchased from Cambridge Isotope Laboratory. Compounds **2**–**3** (48) and **8** (49) were prepared according to the published procedures. NMR spectra were recorded with a Bruker Avance DMX 500 spectrophotometer or a Bruker Avance DMX 400 spectrophotometer with use of the deuterated solvent as the lock and the residual solvent or TMS as the internal reference. ^{1}H and ^{13}C NMR chemical shifts are reported relative to residual solvent signals, and ^{31}P{^{1}H} NMR chemical shifts are referenced to an external unlocked sample of 85% H_3PO_4 (δ 0.0). The 2D DOSY NMR spectra were recorded on a Bruker DRX500 spectrometer. DLS was carried out on a Malvern Nanosizer S instrument at room temperature. Mass spectra were recorded on a Micromass Quattro II triple-quadrupole mass spectrometer using ESI and analyzed using the MassLynx software suite. UV-visible spectra were collected on a Shimadzu UV-2550 UV-visible spectrophotometer. The fluorescence data were measured on an RF-5301 spectrofluorophotometer (Shimadzu Corporation). TEM investigations were carried out on a JEM-1200EX instrument. The samples for TEM experiments (Fig. 6, *A* and *B*) were prepared by placing one drop of a dichloromethane solution of DMC **4** (or **5**) onto a carbon-coated grid and then drying under an infrared light before observation. The samples for TEM experiments (Fig. 6, *C* and *D*) were prepared by placing one drop of a dichloromethane solution of MSP **6** (or **7**) onto a carbon-coated grid, followed by drying under an infrared light before observation. The melting points were collected on a SHPSIC WRS-2 automatic melting point apparatus.

The formation of the discrete metallacycles was achieved by mixing *Z*-**1** with either **2** or **3** in a 1:1 ratio in a 2-dram vial. The solids were dissolved in CH_2Cl_2 and allowed to stir at room temperature for 8 h. To the resulting homogeneous solution, diethyl ether was added to precipitate the product, which was then isolated and dried under reduced pressure for 4 h and redissolved in CD_2Cl_2 for characterization.

DMC **4**: ^{1}H NMR (CD_2Cl_2, room temperature, 500 MHz) δ (ppm): 8.50 (d, J = 5.5 Hz, 8H), 7.68 (d, J = 5.5 Hz, 8H), 7.57 (s, 4H), 7.16 (d, J = 8.5 Hz, 4H), 6.92 (s, 8H), 6.76–6.83 (m, 4H), 5.29 (s, 8H), 2.83 (t, J = 6.3 Hz, 8H), 2.72 (t, J = 6.3 Hz, 8H), 1.12–1.30 (m, 48H), 0.89–1.06 (m, 72H). The ^{31}P{^{1}H} NMR spectrum of metallacycle **4** is shown in *SI Appendix*, Fig. S5. ^{31}P{^{1}H} NMR (CD_2Cl_2, room temperature, 202.3 MHz) δ (ppm): 12.79 ppm (s, ^{195}Pt satellites, $^1J_{Pt-P}$ = 2,725.0 Hz). ESI-MS is shown in *SI Appendix*, Fig. S6: *m/z* 692.26 $[M - 4OTf]^{4+}$, 702.77 $[M - 3OTf - HOTf + K]^{4+}$, 986.67 $[M - 2OTf - HOTf + K]^{3+}$, 1,534.47 $[M - 2OTf]^{2+}$, 1,554.48 $[M - OTf - HOTf + K]^{2+}$.

DCM **5**: ^{1}H NMR (CD_2Cl_2, room temperature, 500 MHz) δ (ppm): 8.52 (d, J = 5.0 Hz, 8H), 7.70 (d, J = 5.0 Hz, 8H), 7.59(s, 4H), 7.29 (s, 16H), 7.17 (d, J = 10.0 Hz, 4H), 6.81–6.83 (m, 4H), 5.32 (s, 8H), 2.84 (t, J = 6.3 Hz, 8H), 2.72 (t, J = 6.3 Hz, 8H), 1.15–1.28 (m, 48H), 0.94–1.06 (m, 72H). The ^{31}P{^{1}H} NMR spectrum of metallacycle **5** is shown in *SI Appendix*, Fig. S8. ^{31}P{^{1}H} NMR (CD_2Cl_2, room temperature, 202.3 MHz) δ (ppm): 13.49 ppm (s, ^{195}Pt satellites, $^1J_{Pt-P}$ = 2692.6 Hz). ESI-MS is shown in *SI Appendix*, Fig. S9: *m/z* 730.77 $[M - 4OTf]^{4+}$, 740.78 $[M - 3OTf - HOTf + K]^{4+}$, 1,037.69 $[M - 2OTf - HOTf + K]^{3+}$, 1,610.50 $[M - 2OTf]^{2+}$, 1,630.51 $[M - OTf - HOTf + K]^{2+}$.

ACKNOWLEDGMENTS. This work was supported by National Basic Research Program Grant 2013CB834502 and National Natural Science Foundation of China Grant 21125417 (to F.H.), National Science Foundation Grant 1212799 (to P.J.S.), and National Natural Science Foundation of China Grants 21222210 and 91027041 (to Q.-Z.Y.).

1. Dublin SN, Conticello VP (2008) Design of a selective metal ion switch for self-assembly of peptide-based fibrils. *J Am Chem Soc* 130(1):49–51.
2. Kudernac T, et al. (2011) Electrically driven directional motion of a four-wheeled molecule on a metal surface. *Nature* 479(7372):208–211.
3. Yan X, Wang F, Zheng B, Huang F (2012) Stimuli-responsive supramolecular polymeric materials. *Chem Soc Rev* 41(18):6042–6065.
4. Göstl R, Senf A, Hecht S (2014) Remote-controlling chemical reactions by light: Towards chemistry with high spatio-temporal resolution. *Chem Soc Rev* 43(6): 1982–1996.
5. Hosono N, et al. (2010) Large-area three-dimensional molecular ordering of a polymer brush by one-step processing. *Science* 330(6005):808–811.
6. Huang Z, Boulatov R (2011) Chemomechanics: Chemical kinetics for multiscale phenomena. *Chem Soc Rev* 40(5):2359–2384.
7. Yang QZ, et al. (2009) A molecular force probe. *Nat Nanotechnol* 4(5):302–306.
8. Xu JF, et al. (2013) Photoresponsive hydrogen-bonded supramolecular polymers based on a stiff stilbene unit. *Angew Chem Int Ed Engl* 52(37):9738–9742.
9. Stang PJ, Olenyuk B (1997) Self-assembly, symmetry, and molecular architecture: Coordination as the motif in the rational design of supramolecular metallacyclic polygons and polyhedra. *Acc Chem Res* 30(12):502–518.
10. Leininger S, Olenyuk B, Stang PJ (2000) Self-assembly of discrete cyclic nanostructures mediated by transition metals. *Chem Rev* 100(3):853–908.
11. Seidel SR, Stang PJ (2002) High-symmetry coordination cages via self-assembly. *Acc Chem Res* 35(11):972–983.
12. Gianneschi NC, Masar MS, 3rd, Mirkin CA (2005) Development of a coordination chemistry-based approach for functional supramolecular structures. *Acc Chem Res* 38(11):825–837.
13. Fujita M, Tominaga M, Hori A, Therrien B (2005) Coordination assemblies from a Pd (II)-cornered square complex. *Acc Chem Res* 38(4):369–378.
14. Oliveri CG, Ulmann PA, Wiester MJ, Mirkin CA (2008) Heteroligated supramolecular coordination complexes formed *via* the halide-induced ligand rearrangement reaction. *Acc Chem Res* 41(12):1618–1629.
15. Northrop BH, Zheng YR, Chi KW, Stang PJ (2009) Self-organization in coordination-driven self-assembly. *Acc Chem Res* 42(10):1554–1563.
16. De S, Mahata K, Schmittel M (2010) Metal-coordination-driven dynamic heteroleptic architectures. *Chem Soc Rev* 39(5):1555–1575.
17. Kreno LE, et al. (2012) Metal-organic framework materials as chemical sensors. *Chem Rev* 112(2):1105–1125.
18. Chakrabarty R, Mukherjee PS, Stang PJ (2011) Supramolecular coordination: Self-assembly of finite two- and three-dimensional ensembles. *Chem Rev* 111(11): 6810–6918.
19. Smulders MM, Riddell IA, Browne C, Nitschke JR (2013) Building on architectural principles for three-dimensional metallosupramolecular construction. *Chem Soc Rev* 42(4):1728–1754.
20. Cook TR, Zheng YR, Stang PJ (2013) Metal-organic frameworks and self-assembled supramolecular coordination complexes: Comparing and contrasting the design, synthesis, and functionality of metal-organic materials. *Chem Rev* 113(1):734–777.
21. Yang HB, et al. (2007) A highly efficient approach to the self-assembly of hexagonal cavity-cored tris[2]pseudorotaxanes from several components *via* multiple noncovalent interactions. *J Am Chem Soc* 129(46):14187–14189.
22. Li S, et al. (2013) Formation of [3]catenanes from 10 precursors *via* multicomponent coordination-driven self-assembly of metallarectangles. *J Am Chem Soc* 135(6):2084–2087.
23. Pluth MD, Bergman RG, Raymond KN (2009) Proton-mediated chemistry and catalysis in a self-assembled supramolecular host. *Acc Chem Res* 42(10):1650–1659.
24. Inokuma Y, Kawano M, Fujita M (2011) Crystalline molecular flasks. *Nat Chem* 3(5): 349–358.
25. Cook TR, Vajpayee V, Lee MH, Stang PJ, Chi KW (2013) Biomedical and biochemical applications of self-assembled metallacycles and metallacages. *Acc Chem Res* 46(11): 2464–2474.
26. Yan X, et al. (2013) Hierarchical self-assembly: Well-defined supramolecular nanostructures and metallohydrogels *via* amphiphilic discrete organoplatinum(II) metallacycles. *J Am Chem Soc* 135(38):14036–14039.
27. Zhao L, Northrop BH, Stang PJ (2008) Supramolecule-to-supramolecule transformations of coordination-driven self-assembled polygons. *J Am Chem Soc* 130(36):11886–11888.
28. Chen S, Chen LJ, Yang HB, Tian H, Zhu W (2012) Light-triggered reversible supramolecular transformations of multi-bisthienylethene hexagons. *J Am Chem Soc* 134(33):13596–13599.
29. Fouquey C, Lehn JM, Levelut AM (1990) Molecular recognition directed self-assembly of supramolecular liquid crystalline polymers from complementary chiral components. *Adv Mater* 2(5):254–257.
30. De Greef TFA, et al. (2009) Supramolecular polymerization. *Chem Rev* 109(11):5687–5754.
31. Sijbesma RP, et al. (1997) Reversible polymers formed from self-complementary monomers using quadruple hydrogen bonding. *Science* 278(5343):1601–1604.
32. Park T, Zimmerman SC (2006) Formation of a miscible supramolecular polymer blend through self-assembly mediated by a quadruply hydrogen-bonded heterocomplex. *J Am Chem Soc* 128(35):11582–11590.
33. Niu Z, Gibson HW (2009) Polycatenanes. *Chem Rev* 109(11):6024–6046.
34. Liu Y, Yu Y, Gao J, Wang Z, Zhang X (2010) Water-soluble supramolecular polymerization driven by multiple host-stabilized charge-transfer interactions. *Angew Chem Int Ed Engl* 49(37):6576–6579.
35. Wang F, et al. (2010) Metal coordination mediated reversible conversion between linear and cross-linked supramolecular polymers. *Angew Chem Int Ed Engl* 49(6): 1090–1094.
36. Niu Z, Huang F, Gibson HW (2011) Supramolecular AA-BB-type linear polymers with relatively high molecular weights *via* the self-assembly of bis(*m*-phenylene)-32-crown-10 cryptands and a bisparaquat derivative. *J Am Chem Soc* 133(9):2836–2839.
37. Gröger G, et al. (2011) Switchable supramolecular polymers from the self-assembly of a small monomer with two orthogonal binding interactions. *J Am Chem Soc* 133(23): 8961–8971.
38. Folmer BJB, Sijbesma RP, Verseegen RM, van der Rijt JAJ, Meijer EW (2000) Supramolecular polymer materials: chain extension of telechelic polymers using a reactive hydrogen-bonding synthon. *Adv Mater* 12(12):874–878.
39. Burnworth M, et al. (2011) Optically healable supramolecular polymers. *Nature* 472(7343):334–337.
40. Yan X, et al. (2012) A multiresponsive, shape-persistent, and elastic supramolecular polymer network gel constructed by orthogonal self-assembly. *Adv Mater* 24(3): 362–369.
41. Aida T, Meijer EW, Stupp SI (2012) Functional supramolecular polymers. *Science* 335(6070):813–817.
42. Ji X, Yao Y, Li J, Yan X, Huang F (2013) A supramolecular cross-linked conjugated polymer network for multiple fluorescent sensing. *J Am Chem Soc* 135(1):74–77.
43. Zhang M, et al. (2012) Self-healing supramolecular gels formed by crown ether based host-guest interactions. *Angew Chem Int Ed Engl* 51(28):7011–7015.
44. Yan X, et al. (2013) Supramolecular polymers with tunable topologies via hierarchical coordination-driven self-assembly and hydrogen bonding interfaces. *Proc Natl Acad Sci USA* 110(39):15585–15590.
45. Yan X, et al. (2013) Dendronized organoplatinum(II) metallacyclic polymers constructed by hierarchical coordination-driven self-assembly and hydrogen-bonding interfaces. *J Am Chem Soc* 135(45):16813–16816.
46. Yan X, et al. (2014) Responsive supramolecular polymer metallogel constructed by orthogonal coordination-driven self-assembly and host/guest interactions. *J Am Chem Soc* 136(12):4460–4463.
47. Qu DH, Feringa BL (2010) Controlling molecular rotary motion with a self-complexing lock. *Angew Chem Int Ed Engl* 49(6):1107–1110.
48. Manna J, et al. (1997) Nanoscale tectonics: Self-assembly, characterization, and chemistry of a novel class of organoplatinum square macrocycles. *J Am Chem Soc* 119(48): 11611–11619.
49. Akbulatov S, Tian Y, Boulatov R (2012) Force-reactivity property of a single monomer is sufficient to predict the micromechanical behavior of its polymer. *J Am Chem Soc* 134(18):7620–7623.